Novel one step hydrothermal synthesis of TiO_2/WO_3 nanocomposites with enhanced photocatalytic activity†

Valeria Puddu,[a] Robert Mokaya[b] and Gianluca Li Puma*[a]

Received (in Cambridge, UK) 30th July 2007, Accepted 29th August 2007
First published as an Advance Article on the web 7th September 2007
DOI: 10.1039/b711559h

A novel and simple one step hydrothermal process is used to prepare TiO_2/WO_3 nanocomposites, in which WO_3 and TiO_2 are present in hexagonal and anatase crystalline forms, respectively, and have enhanced photocatalytic activity towards trichloroethylene degradation in the gas phase.

Coupling TiO_2 with other metal oxides (*e.g.*, WO_3 or V_2O_5) is an approach that has received much attention for improving the photocatalytic properties of TiO_2.[1–8] The absorption of photons with an energy equal to or higher than the TiO_2 semiconductor bandgap (E_g) gives rise to photoexcited electron–hole pairs. Electron–hole pairs can initiate redox reactions with adsorbates at the catalyst surface or can result in their recombination with the release of heat. These two processes compete, and one of the key factors that controls the efficiency of a photocatalyst is the electron/hole recombination rate, as it controls the availability of photoexcited sites on the catalyst surface. When anatase TiO_2 (E_g = 3.2 eV) is doped with a semiconductor of smaller bandgap, such as WO_3 (E_g = 2.8 eV), improved charge separation can result from the coupling of the two materials.[2] W(VI) in WO_3 is considered to act as trapping site by accepting the photoexcited electrons from the TiO_2 valence band, hence generating W(V).[3] The electron in W(V) can then be transferred to surface reducible species. Moreover, since WO_3 exhibits a higher acidity than TiO_2, its presence in the nanocomposite can modify the affinity of substrates for the catalyst surface, and as a consequence, the adsorption equilibrium and photooxidation activity of the catalyst.[3]

The addition of WO_3 to TiO_2 has been observed to improve the photooxidation of butyl acetate,[4] benzene,[3] 2-propanol[3] and toluene[5] in the vapor phase. WO_3-doped TiO_2 photocatalysts have, so far, been prepared using only two step procedures by sol–gel,[6,8,9] impregnation,[1,10] microemulsion,[5] hydrothermal[11] and mechanical[12] methods. In all of these synthetic methods, an amorphous precursor is first obtained (step 1), then a thermal treatment at relatively high temperatures (step 2) is carried out to permit the formation of the final photoactive crystalline material.

In this communication, we describe a new synthetic approach based on a hydrothermal process that leads to photoactive TiO_2/WO_3 nanocomposites. This synthesis method is based on a simple "one step" hydrothermal reaction, where $TiOSO_4$ and ammonium metatungstate ($(NH_4)_6(W_{12}O_{41})\cdot xH_2O$) are used as precursors for TiO_2 and WO_3, respectively. In a typical synthesis, appropriate amounts of each precursor were mixed with 100 ml of H_2O and ethanol in a 1 : 1 ratio in a 150 ml autoclave Teflon vessel and reacted hydrothermally at 150 °C for 12 h. The reaction powder obtained was filtered and washed twice with water, ethanol and acetone, then dried at room temperature overnight. The percentage of WO_3 in the nanocomposites was varied between 1 and 40% wt. For comparison purposes, TiO_2 and WO_3 were also prepared by following the same protocol as for the mixed oxides. Each sample was prepared twice to assure consistency in the preparation method.

Fig. 1 shows the XRD patterns of the nanocomposites. The XRD reveals that TiO_2 is present in the anatase form in all samples. The WO_3 has been identified with $(NH_4)_{0.33}WO_3$ (JCPDS 42-0452) in a hexagonal form, which contrasts with the orthorhombic WO_3 ($WO_3\cdot0.33\ H_2O$) and monoclinic WO_3 obtained by Kominami *et al.*[13] following hydrothermal treatment at 473 and 523 K, respectively, using a KH_2WO_4 precursor. All other TiO_2/WO_3 nanocomposites exhibit WO_3 in a hexagonal form.

The structural properties of the nanocomposites were measured from duplicate XRD and N_2 adsorption–desorption analyses, and the results are reported in Table 1. The anatase crystallite size was found to be in the range 18–30 nm. The WO_3 loading was found to affect the size of the anatase crystals in the nanocomposites with an

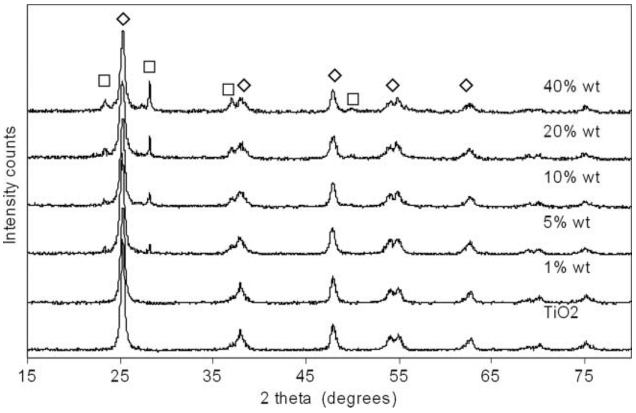

Fig. 1 XRD patterns of TiO_2/WO_3 nanocomposites (□ = WO_3, ◇ = TiO_2).

---

[a] *Photocatalysis & Photoreaction Engineering, School of Chemical and Environmental Engineering, The University of Nottingham, University Park, Nottingham, UK NG7 2RD.*
E-mail: gianluca.li.puma@nottingham.ac.uk; Fax: +44 115 9514115; Tel: +44 115 9514170
[b] *School of Chemistry, The University of Nottingham, University Park, Nottingham, UK NG7 2RD. E-mail: r.mokaya@nottingham.ac.uk; Fax: +44 115 9513562; Tel: +44 115 8466174*

† Electronic supplementary information (ESI) available: N_2 sorption isotherms, SEM images and a description of the photocatalytic reactor. See DOI: 10.1039/b711559h

Table 1 Textural properties of TiO_2 samples with different WO_3 contents

WO_3 (% wt)	$D_{anatase}$^{a}/nm	SSA^b/m^2 g^{-1}	V_{pore}^{c}/cm^3 g^{-1}
0	30	100	0.30
1	28	86	0.17
5	26	87	0.21
10	23	136	0.22
20	21	102	0.24
40	18	99	0.20
100	—	7.6	—

[a] Diameter calculated from the broadening of the (101) anatase peak using Scherrer's equation. [b] Specific surface area determined using the BET method in the range $0.05 < P/P_0 < 0.35$. [c] BJH desorption pore volume calculated between 2 and 300 nm.

inverse relationship. The WO_3 loading did not significantly affect the porosity properties of the mixed oxides (*i.e.*, pore size and pore volume).

Fig. 2 shows the N_2 sorption isotherm of pure TiO_2, pure WO_3 and the nanocomposite with 20% wt WO_3. Isotherms similar to that of the 20% wt sample were observed for the other mixed oxide nanocomposites (ESI Fig. S1†). The isotherm of pure WO_3 matches that of a typical Type II (BDDT classification), which is usually attributed to non-porous materials or materials of very limited porosity. In contrast, pure TiO_2 and the mixed oxide samples present isotherms indicative of significant porosity. The N_2 sorption isotherms may generally be classified as Type IV, with an inflection and hysteresis loop in the relative pressure $P/P_0 > 0.3$. The isotherms suggest that the porosity of the mixed oxide nanocomposites is very similar to that of pure TiO_2; both types of material have a relatively wide pore size distribution in the mesopore size range. At relative pressures approaching $P/P_0 = 0.3$, the pure TiO_2 and nanocomposites exhibit significant sorption, which we attribute to the presence of large pores or macropores arising from interparticle voids. The higher pore volume of the pure TiO_2 (Table 1) may, in part, be due to the presence of more interparticle voids.

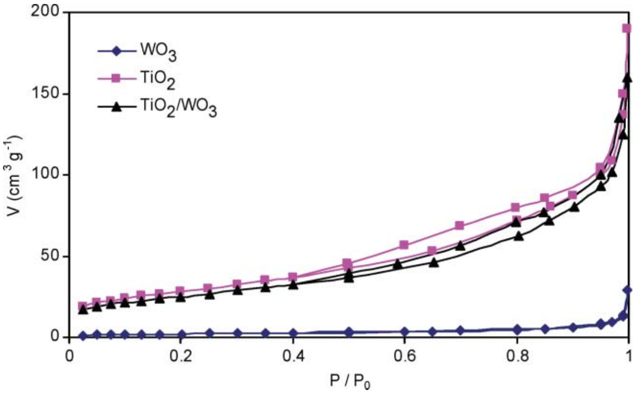

Fig. 2 N_2 adsorption–desorption isotherms of pure Ti and W oxides, and of a TiO_2/WO_3 nanocomposite with 20% wt WO_3.

The SEM images shown in Fig. 3 (and ESI Fig. S2†), providing visualisation of the textural properties of large portions of samples, indicate that the pure TiO_2 is made up of irregularly-shaped aggregates with sizes between 0.1 and 1 μm. The particles generally

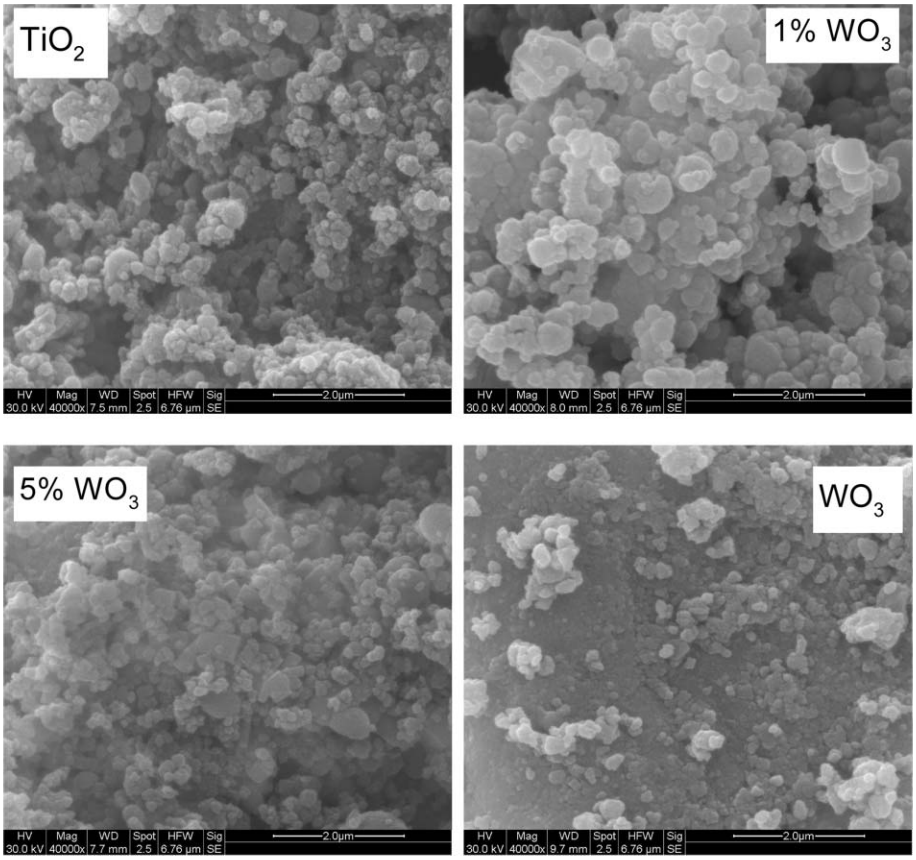

Fig. 3 SEM images of pure TiO_2, pure WO_3 and mixed TiO_2/WO_3 samples.

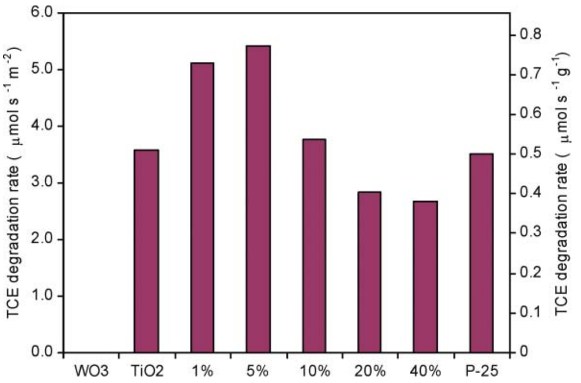

Fig. 4 Reaction rates of TiO_2 samples having different WO_3 contents. Reaction rates are per unit surface area of irradiated coated support (left axis) and per unit weight of supported catalyst (right axis).

exist in loose aggregates with a significant quantity of interparticle voids, which is consistent with the sorption data. Addition of WO_3 does not significantly affect the particle morphology, except for a slight increase in the level of particle aggregation and an associated decrease in interparticle voids. The sample with 10% WO_3 shows a peculiar behavior, with a morphological structure similar to that of pure TiO_2 (ESI Fig. S2†), but with a slight increase in porosity, which corroborates with an increase in surface area (Table 1). Conversely, pure WO_3 exhibits a highly aggregated particle morphology, which may explain the lower level of interparticle voids evident from the sorption data.

The photocatalytic activity of the nanocomposites were evaluated by measuring the rate of decomposition of trichloroethylene (TCE) in air in the presence of water vapour. The nanocomposite powders were deposited on silica glass plates (area 75 cm^2) from ethanolic suspensions, achieving a catalyst loading of 0.7 mg cm^{-2} for all supports. A narrow slit, flat-plate, single-pass, flow-through photocatalytic reactor was used. A short description and diagram of the reactor is shown in the ESI (Fig. S3).† Further specification details are reported elsewhere.[14] The experiments were conducted in a reaction-controlled regime using a total flow rate of 0.04 L s^{-1}, 8% relative humidity, an initial concentration of TCE in synthetic air (20% O_2, 80% N_2; BOC gases) of 24.8 ± 2 µM and an incident photon flux on the supported catalyst of 5.53 W m^{-2} (UVA). Experiments were carried out under "differential reactor" conditions (TCE conversions $< 10\%$) to permit estimation of the reaction rate from the conversion of TCE at steady-state. Reaction rates of the mixed oxide samples were compared to those of single component catalysts evaluated under the same conditions, and with that of commercial TiO_2 Degussa P-25 reference catalyst.

No TCE degradation was detected in the dark or in the absence of catalyst. Therefore, all variation in TCE concentration was ascribed to the photocatalytic activity of the catalyst. The results are shown in Fig. 4. Pure WO_3 did not show any photocatalytic activity towards TCE under the operating conditions used. The activity of the hydrothermal TiO_2 sample was similar to that of P-25. The nanocomposites with WO_3 contents of 1–5% wt showed up to 42% higher photocatalytic activity compared to that of TiO_2, despite having a lower surface area (Table 1). The enhancement in the rate can therefore be attributed to improved charge separation. However, at WO_3 loadings of 10% wt or higher, the activity reduced as a result of the dilution effect of the inactive WO_3 phase.

In conclusion, the one step hydrothermal method reported here for the preparation of TiO_2/WO_3 nanocomposites in singular crystalline forms resulted in materials with enhanced photoactivity compared to TiO_2 alone. The photocatalytic activities were higher than commercial Degussa P-25 for samples with loadings of up to 5% wt WO_3, possibly due to the coupling effect of the two semiconductors and enhanced charge separation.

To the best of our knowledge, this is the first time that a hexagonal form of WO_3 has been reported in a hydrothermally-prepared nanocomposite that shows enhanced photocatalytic activity. Further work on the optimisation of the synthesis conditions, and a detailed elucidation of the role of the synthesis parameters on the structural properties and photocatalytic activity is currently under way.

Financial support from the EPSRC (Grant GR/S77875) is gratefully acknowledged.

Notes and references

1 P. Avila, A. Bahamonde, J. Blanco, B. Sánchez, A. I. Cardona and M. Romero, *Appl. Catal., B*, 1998, **30**, 75.
2 G. Marci, L. Palmisano, A. Sclafani, A. M. Venezia, R. Campostrini, G. Carturan, C. Martin, V. Rives and G. Solana, *J. Chem. Soc., Faraday Trans.*, 1996, **92**, 819 and references therein.
3 Y. T. Kwon, K. Y. Song, W. I. Lee, G. J. Choi and Y. R. Do, *J. Catal.*, 2000, **191**, 192.
4 V. Keller, P. Bernhardt and F. Garin, *J. Catal.*, 2003, **215**, 129.
5 A. Fuerte, M. D. Hernández-Alonso, A. J. Maira, A. Martínez-Arias, M. Fernández-García, J. C. Conesa, J. Soria and G. Munuera, *J. Catal.*, 2002, **212**, 1.
6 H. Yang, R. Shi, K. Zhang, Y. Hu, A. Tang and X. Li, *J. Alloys Compd.*, 2005, 200.
7 A. Rampaul, I. P. Parkin, S. A. O'Neill, J. DeSouza, A. Mills and N. Elliot, *Polyhedron*, 2003, **22**, 35.
8 J. Georgieva, S. Armyanov, E. Valova, I. Poulios and S. Sotiropoulos, *Electrochem. Commun.*, 2007, **9**, 365.
9 H. Yang, D. Zhang and L. Wang, *Mater. Lett.*, 2002, **57**, 674.
10 G. M. Zuo, Z. X. Cheng, H. Chen, G. W. Li and T. Miao, *J. Hazard. Mater.*, 2006, **128**, 158.
11 D. Ke, H. Liu, T. Peng, X. Liu and K. Dai, *Mater. Lett.*, 2007, DOI: 10.1016/j.matlet.2007.05.060.
12 C. Shifu, C. Lei, G. Shen and C. Gengyu, *Powder Technol.*, 2005, **160**, 198.
13 H. Kominami, J. I. Kato, S. Y. Murakami, Y. Ishii, M. Kohno, K. I. Yabutani, T. Yamamoto, Y. Kera, M. Inoue, T. Inui and B. Ohtani, *Catal. Today*, 2003, **84**, 181.
14 I. Salvado-Estivill, D. M. Hargreaves and G. Li Puma, *Environ. Sci. Technol.*, 2007, **41**, 2028.